ELSEVIER

Comput. Methods Appl. Mech. Engrg. 157 (1998) 365–385

Computer methods in applied mechanics and engineering

Thermal generalized stress intensity factors in 2-D domains

Zohar Yosibash

Pearlstone Center for Aeronautical Engineering Studies, Dept. of Mechanical Engineering, Ben-Gurion University of the Negev, Beer-Sheva 84105, Israel

Received 22 November 1996

Abstract

Computation of thermal generalized stress intensity factors (TGSIFs) in linear thermo-elastic two-dimensional problems with singular points subjected to steady-state temperature distribution is addressed. The stress tensor in the vicinity of singular points exhibits singular behavior characterized by the strength of the singularity and the associated TGSIFs. The p-version of the finite element method is first used to compute the temperature field, usually exhibiting singular behavior of the fluxes in the vicinity of the singular point, then imposed in the elastic analysis as thermal loading, exciting the TGSIFs. A post-processing technique based on the complementary weak form in conjunction with Richardson extrapolation is applied to extract the TGSIFs. Importantly, the proposed method is applicable, not only to singularities associated with crack tips, but also to multi-material interfaces and non-homogeneous materials. Numerical results of crack-tip singularities (mode I, mode II and mixed modes) and singular points associated with a two-material inclusion and a 90° dissimilar materials wedge, are presented.

1. Introduction

Lately, methods that are capable of predicting failure initiation and propagation in structural components subjected to thermal loads are sought. It is postulated, as in the theory of linear elastic fracture mechanics, that the methods should correlate experimental observed failures to parameters characterizing the thermo-elastic stress field in the vicinity of failure initiation points. Failures due to thermal loading occur, for example, in integrated circuits which are assemblages of dissimilar materials with different thermal and mechanical properties. The mismatch of elastic constants and thermal expansion coefficients causes stress intensification at corners of interfaces and may lead to mechanical failure. These corners as well as crack tips are called singular points because the stress tensor is infinity in the linear theory of elasticity, and so are the steady-state temperature fluxes if the temperature field is influenced by the presence of the discontinuity in geometry or thermal properties.

New approaches for predicting the initiation and extension of de-laminations in plastic-encapsulated LSI (Large Scale Integrated Circuit) devices, for example, are based on the computation of the thermal generalized stress intensity factors (TGSIFs) and the strength of the stress singularity [1,2]. The TGSIFs are the first two coefficients of the asymptotic expansion of the stress tensor in the vicinity of the singular point, and the strength of the stress singularity characterizes how fast the stress tensor approaches infinity in the vicinity of the singular point.

Although many studies were reported in the past 30 years on thermo-elastic crack problems in isotropic two-dimensional domains (see e.g. [3–5] and the references therein), very little has been done on multi-material corner interfaces. Especially, scant attention has been given to singularities affecting both the temperature flux field and the stress tensor. Recent publications on TGSIFs for bonded interface between dissimilar materials, ignoring the singular behavior of the temperature fluxes, can be found for example in [1,6–8] and the references therein. To the best of our knowledge no previous numerical or rigorous analytical treatment is available on

0045-7825/98/$19.00
PII S0045-7825(97)00246-6

singularities affecting both the temperature flux and the stress field, and also applicable to isotropic as well as anisotropic multi-material interfaces.

Herein, the un-coupled linear heat-conduction and elasticity theories are applied over two-dimensional domains to reliably compute the TGSIFs and the strength of stress singularity for crack tips and multi-material corner interfaces, taking into consideration the singular behavior of the thermal stress field. Using the p-version of the finite element method, the temperature distribution is first found, which is imposed thereafter as a thermal load in the elasticity problem. The strength of the flux and stress singularities are computed using the modified Steklov method [9]. The complementary weak form is then applied in the post-processing phase over a series of sub-domains with decreasing radii for computing the TGSIFs and by using Richardson extrapolation excellent results are obtained. This extraction procedure is an extension of recently developed methods reported in [9–11] for thermo-elastic problems.

In Sections 2 and 3, the classical and the corresponding complementary weak formulations of thermo-elastic problems is presented. The results of the mathematical analysis are demonstrated in Section 4 by extracting the TGSIFs for several problems involving cracks in rectangular plates and cracks emanating from a circular hole, subjected to different temperature boundary conditions. In Section 5 TGSIFs for dissimilar isotropic elastic wedges perfectly bonded along their common interface, representing inclusion problems and a 90° two wedge interface problem are summarized. The conclusions to be drawn from the calculations, are outlined in Section 6.

2. Classical (strong) formulation of the linear thermo-elastic problem

Notations and preliminaries

Let Ω be a simple connected two-dimensional domain with boundaries $\partial\Omega \cup_i \Gamma_i$ which are analytic simple arc curves called edges. The outward normal vector to the boundary is denoted by $\boldsymbol{n} \overset{\text{def}}{=} (n_1, n_2)$, and in matrix form:

$$[n] = \begin{bmatrix} n_1 & 0 & n_2 \\ 0 & n_1 & n_2 \end{bmatrix}.$$

Assume that Ω contains a reentrant corner, for example, with an internal angle ω, created by the intersection of two straight edges Γ_1 and Γ_2. The intersection point P is called a singular point because the stress tensor in the linear theory of elasticity, and the flux vector in the linear theory of heat conduction is unbounded at this point. A circular domain S_R is defined as the interior points of a circle of radius R centered in the singular point, and we construct a sub-domain Ω_R defined by $\Omega \cap S_R$, see Fig. 1. *In this paper the discussion is concentrated mainly on the solution near the singular point P.* The div operator on vectors and **div**, **grad** operators on tensors in 2-D are defined according to [12, Chap. 9].

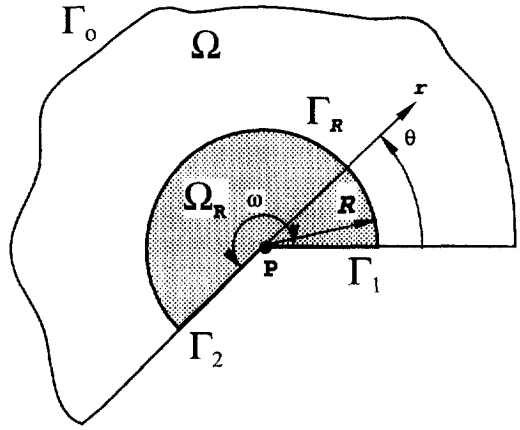

Fig. 1. Domain and notations.

2.1. The linear heat conduction problem

We denote by $\tau(x, y)$ the temperature field, which is the solution of the linear heat conduction problem

$$\operatorname{div}([a]\operatorname{grad}\tau) = 0 \quad \text{in } \Omega \tag{1}$$

with prescribed Dirichlet boundary conditions on a part of $\partial\Omega$, prescribed Neumann boundary condition ($q_n = \operatorname{grad}\tau \cdot \boldsymbol{n}$) on the other part of $\partial\Omega$, and homogeneous boundary conditions on $\Gamma_1 \cup \Gamma_2$. The 2×2 matrix $[a]$ consists of the heat conduction coefficients $a_{11}, a_{22}, a_{12} = a_{21}$, which are assumed to be constants (or piecewise constants in multi-material interface problems) and satisfy the ellipticity restriction. In isotropic materials ($a_{11} = a_{22}$, $a_{12} = 0$) (1) becomes the Laplace equation and the temperature field is independent of $[a]$. The heat conduction problem is solved in practice by means of the p-version of the finite element method (see details in [13, Chap. 8]) over Ω, however, for mathematical analysis purposes it is assumed that the exact solution can be found. In the vicinity of the singular point P, the special functional representation of τ is of special interest in the sequel.

There are two different approaches when considering the temperature field in the vicinity of P. The simplified approach assumes that for crack tips, for example, the presence of a singular point does not influence the heat flow continuum, because the two faces of the crack remain in contact, or are almost in contact (for small deformation elasticity theory). In this case it is assumed that $\tau =$ constant in the vicinity of P.

The other approach, i.e. when the faces $\Gamma_1 \cup \Gamma_2$ are assumed to be either isolated or the temperature is kept constant, the temperature field, is expressed in the vicinity of the singular point as

$$\tau(r, \theta) = \tau_0 + \sum_{i=1}^{\infty}\sum_{s=0}^{S} b_{is} r^{\beta_i} \ln^s(r) h_{is}(\theta)\,, \tag{2}$$

r and θ being the polar co-ordinates of a system located at P, $\beta_i \geqslant 0$ and $\beta_i < \beta_j$ for $i < j$. τ_0 is a constant which may be zero, depending on temperature boundary conditions (except for inclusion problems where it is almost always not zero). The coefficients b_{is}, called generalized flux intensity factor, are uniquely determined by the thermal boundary conditions on $\Gamma_1 \cup \Gamma_2$ and away from the singular point. $S = 1$ only for special angles for which β_i is an integer number, otherwise, $S = 0$ (see [14, p. 264]). If grad τ is considered, the terms containing the ln r functions are less singular than terms containing r^{β_i} for $\beta_i < 1$. The same functional representation given by (2) apply also to multi-material interface domains [15].

2.2. The linear thermo-elasticity problem

Once the linear heat conduction problem is solved over Ω, one may proceed to the un-coupled linear thermo-elasticity problem, and prescribe the exact temperature field as a thermal loading. The displacements vector expressed in a Cartesian coordinate system is denoted by $\boldsymbol{u} \overset{\text{def}}{=} (u_1, u_2)^{\mathrm{T}}$ and the linear strain tensor by

$$\varepsilon_{ij}(\boldsymbol{u}) = \frac{1}{2}\left(\frac{\partial u_i}{\partial x_j} + \frac{\partial u_j}{\partial x_i}\right).$$

Throughout the paper the stress tensor in two dimensions will be denoted either by its tensor or vector form,

$$\underset{\sim}{\boldsymbol{\sigma}} \overset{\text{def}}{=} \begin{bmatrix} \sigma_{11} & \sigma_{12} \\ \sigma_{12} & \sigma_{22} \end{bmatrix} \quad \text{or} \quad \boldsymbol{\sigma} \overset{\text{def}}{=} (\sigma_{11} \quad \sigma_{22} \quad \sigma_{12})^{\mathrm{T}}$$

The constitutive law (Hooke's law) for a two-dimensional elastic material is given by

$$[C]\boldsymbol{\sigma} = \boldsymbol{\varepsilon} \overset{\text{def}}{=} (\varepsilon_{11} \quad \varepsilon_{22} \quad \varepsilon_{12})^{\mathrm{T}} \tag{3}$$

where for an isotropic material

$$[C] = \frac{1+\nu}{2E}\begin{bmatrix} \frac{1}{\delta}+1 & \frac{1}{\delta}-1 & 0 \\ \frac{1}{\delta}-1 & \frac{1}{\delta}+1 & 0 \\ 0 & 0 & 2 \end{bmatrix}, \qquad \delta = \begin{cases} \dfrac{1}{1-2\nu} & \text{plane strain} \\ \dfrac{1+\nu}{1-\nu} & \text{plane stress} \end{cases},$$

and E and ν are the Young's modulus and the Poisson's ratio, respectively. The matrix $[C]$ is fully populated for an anisotropic material. For presentation simplicity we restrict our discussion to isotropic materials, although the present methods are equally applicable to anisotropic materials.

Traction-free boundary conditions are assumed on Γ_1 and Γ_2, thus the boundary conditions (due to thermal loading alone) are

$$t_n = \mu\beta\tau \quad \text{on } \Gamma_1 \cup \Gamma_2, \tag{4}$$

t_n being the normal traction on the boundary, $\mu = E/2(1+\nu)$, τ is the elevated temperature field in respect to the stress-free state,

$$\beta = \begin{cases} \dfrac{2(1+\nu)}{1-2\nu}\alpha & \text{plane strain} \\ \dfrac{2(1+\nu)}{1-\nu}\alpha & \text{plane stress} \end{cases}$$

and α is the coefficient of linear thermal expansion. Again, it is assumed that the thermo-elasticity problem can be solved analytically over Ω for mathematical analysis purposes, but the p-version of the finite-element method is used for performing the actual computations. On the boundary $\Gamma_0 = \partial\Omega - \Gamma_1 - \Gamma_2$, displacement, traction or spring boundary conditions may be applied, however, on Γ_1 and Γ_2 we assume homogeneous mechanical boundary conditions.

Since the focus of this work is the solution of the thermo-elasticity problem in the vicinity of the singular point, we concentrate our attention in the sub-domain Ω_R, assuming that the displacement field on Γ_R is available. The classical linear thermo-elastic problem in an isotropic domain Ω_R described in terms of stresses is

$$\mathbf{div}\ \underset{\sim}{\sigma} = \beta\ \mathrm{grad}\ \tau \quad \text{in } \Omega_R \tag{5}$$

$$t_n = \sigma_{\theta\theta} = \mu\beta\tau \quad \text{on } \Gamma_1 \cup \Gamma_2, \tag{6}$$

$$t_t = \sigma_{r\theta} = 0 \quad \text{on } \Gamma_1 \cup \Gamma_2, \tag{7}$$

$$\boldsymbol{u} \text{ prescribed} \quad \text{on } \Gamma_R.$$

The stress tensor which is the solution to the thermo-elastic problem in the vicinity of the singular point consists of three parts

$\underset{\sim}{\sigma}_P$: a particular stress tensor solution satisfying the partial differential equation (5) and homogeneous boundary conditions on $\Gamma_1 \cup \Gamma_2$.

$\overline{\underset{\sim}{\sigma}}_P$: another particular stress tensor solution which satisfies the *homogeneous* partial differential equation (5), and the boundary conditions (6) and (7).

$\underset{\sim}{\sigma}_H$: a *homogeneous* stress tensor defined by

$$\underset{\sim}{\sigma}_H = \underset{\sim}{\sigma} - \underset{\sim}{\sigma}_P - \overline{\underset{\sim}{\sigma}}_P.$$

Thus, $\underset{\sim}{\sigma}_H$ only involves the ordinary stress singularities as shown in the following:

$\underline{\underset{\sim}{\sigma}_H}$:

The stress tensor which is the solution to the homogeneous equilibrium equations with homogeneous traction boundary conditions in the neighborhood of a singular point can be expanded in an asymptotic series (herein we use the vector representation of the stress tensor)

$$\boldsymbol{\sigma}_H(r,\theta) = \sum_{i=1}^{\infty}\sum_{m=0}^{M} A_{im} r^{\alpha_i - 1} \ln^m r \boldsymbol{F}_{im}(\theta) \tag{8}$$

where A_{im} are the coefficients of the asymptotic expansion (called the *generalized stress intensity factors—GSIFs*). The GSIFs are determined uniquely by the traction and displacement boundary conditions *away from the singular point*, and when excited by thermal loading they are called thermal generalized stress intensity factors (TGSIFs). The first two GSIFs associated with crack tip singularities are called stress intensity factors

(SIFs) in fracture mechanics terminology and are denoted by K_{I} and K_{II}, or thermal stress intensity factors (TSIFs) if they are excited by the thermal loading. The eigenvalues α_i and the eigen-stresses $\boldsymbol{F}_{im}(\theta)$ are associated pairs which depend on material properties, geometry, and boundary conditions *in the vicinity of the singular point only*. Notice that the function vectors $\boldsymbol{F}_{im}(\theta)$ vanish on $\Gamma_1 \cup \Gamma_2$ because homogeneous traction boundary conditions are assumed. The smallest eigenvalue is called the strength of the stress singularity, and $\alpha_i < \alpha_j$ for $i < j$. Under special (exeptional) circumstances, for specific combination of material properties and geometry, $M \neq 0$. However, we restrict our discussion to cases where $M = 0$, thus (8) to be addressed is

$$\boldsymbol{\sigma}_{\mathrm{H}}(r,\theta) = \sum_{i=1}^{\infty} A_i r^{\alpha_i - 1} \boldsymbol{F}_i(\theta)\,. \tag{9}$$

This displacements vector corresponding to (9) is given by

$$\boldsymbol{u}_{\mathrm{H}}(r,\theta) = \sum_{i=1}^{\infty} A_i r^{\alpha_i} \boldsymbol{f}_i(\theta)\,, \tag{10}$$

where $\boldsymbol{f}_i(\theta)$ are the eigen-functions of the so-called homogeneous solution.

$\underline{\underline{\boldsymbol{\sigma}}}_{\mathrm{P}}$ *and* $\underline{\underline{\bar{\boldsymbol{\sigma}}}}_{\mathrm{P}}$:

Both particular stress tensors $\underline{\underline{\boldsymbol{\sigma}}}_{\mathrm{P}}$ and $\underline{\underline{\bar{\boldsymbol{\sigma}}}}_{\mathrm{P}}$ depend on the temperature field τ in the vicinity of the singular point. These particular stress tensors do not play a direct role in the numerics, and do not have to be actually computed. Their main role is the linkage to the theoretical framework providing the justification of their removal in a systematic way.

As mentioned in Subsection 2.1, the simplified approach is to assume that the singular point has negligible influence on the distribution of the temperature in its vicinity. Therefore, the temperature distribution in the *closed vicinity of the crack tip* may be considered to be constant. In this case the thermo-elasticity problem to be solved becomes

$$\mathbf{div}\ \underline{\underline{\boldsymbol{\sigma}}} = \beta\ \mathrm{grad}\ \tau = 0 \quad \text{in } \Omega_R \tag{11}$$

$$t_n = \sigma_{\theta\theta} = \mu\beta\tau = C \quad \text{on } \Gamma_1 \cup \Gamma_2\,, \tag{12}$$

$$t_t = \sigma_{r\theta} = 0 \quad \text{on } \Gamma_1 \cup \Gamma_2\,. \tag{13}$$

The solution to the problem (11), (12) and (13) consists of two parts only

$$\underline{\underline{\boldsymbol{\sigma}}} = \underline{\underline{\boldsymbol{\sigma}}}_{\mathrm{H}} + \underline{\underline{\bar{\boldsymbol{\sigma}}}}_{\mathrm{P}}\,.$$

A particular stress tensor $\underline{\underline{\bar{\boldsymbol{\sigma}}}}_{\mathrm{P}}$ which satisfies the equilibrium equations (11), and the boundary conditions (12) and (13) is

$$(\bar{\sigma}_{rr} \quad \bar{\sigma}_{\theta\theta} \quad \bar{\sigma}_{r\theta})^{\mathrm{T}}_{\mathrm{P}} = \begin{Bmatrix} C \\ C \\ 0 \end{Bmatrix} \overset{\mathrm{def}}{=} \boldsymbol{\sigma}_o\,. \tag{14}$$

The second approach of considering the temperature field assumes that the temperature field is disturbed by the singular point. In this case the temperature flux posses singular behavior in the vicinity of the singular point and the temperature field is given by (2). It is assumed that $\beta_1 \neq \alpha_i - 1$ for any i and $\beta_1 < 1$. By separation of variables, using the shift theorem for the equation in r, the stress vector $\boldsymbol{\sigma}_{\mathrm{P}}$ in the vicinity of the singular point can be represented as follows:

$$\boldsymbol{\sigma}_{\mathrm{P}}(r,\theta) = \boldsymbol{\sigma}_o + B r^{\beta_1} \boldsymbol{H}(\theta) + \mathcal{O}(r^{\beta_1 + \epsilon}) \tag{15}$$

where B is a constant, and $\epsilon > 0$. If $\beta_1 = \alpha_i - 1$, then (16) will also contain a $\ln(r)$ term

$$\boldsymbol{\sigma}_{\mathrm{P}}(r,\theta) = \boldsymbol{\sigma}_o + B r^{\beta_1} \ln(r) \boldsymbol{F}_i(\theta) + r^{\beta_1} \boldsymbol{H}(\theta) + \mathcal{O}(r^{\beta_1 + \epsilon}) \tag{16}$$

where B is chosen so as to satisfy Fredholm's Alternative (see [16, pp. 78–80]). This case is not addressed in the following.

Since $\underset{\sim}{\boldsymbol{\sigma}}_{\mathrm{P}}$ vanishes on the boundaries $\Gamma_1 \cup \Gamma_2$, the stress tensor $\overline{\underset{\sim}{\boldsymbol{\sigma}}}$ can be any tensor that produces only non-zero $\sigma_{\theta\theta}$ and this could be a linear function of θ multiplied by a function of r of the form $r^{\beta_1} + \mathcal{O}(r^{\beta_1+\epsilon})$.

The displacements vector corresponding to $\underset{\sim}{\boldsymbol{\sigma}}_{\mathrm{P}} + \overline{\underset{\sim}{\boldsymbol{\sigma}}}_{\mathrm{P}}$ is denoted by $\boldsymbol{u}_{\mathrm{P}}$ and can be expressed in the vicinity of the singular point (as $r \to 0$) by

$$\boldsymbol{u}_{\mathrm{P}}(r, \theta) = \boldsymbol{u}_o + r\boldsymbol{g}(\theta) + \mathcal{O}(r^{\beta_1+1+\epsilon}), \tag{17}$$

where $\boldsymbol{u}_o$ is a vector containing constants (describing the displacements of the singular point P), and $\boldsymbol{g}(\theta)$ is an analytic vector function of θ.

3. The weak complementary formulation of the thermo-elastic problem

Let $\underset{\sim}{\boldsymbol{\Sigma}}(\Omega_R)$ be the statically admissible space defined by

$$\underset{\sim}{\boldsymbol{\Sigma}}(\Omega_R) = \{\underset{\sim}{\boldsymbol{\sigma}} \mid \|\underset{\sim}{\boldsymbol{\Sigma}}\|_{L^2,\Omega_R} < \infty; \ \mathbf{div}\ \underset{\sim}{\boldsymbol{\sigma}} = \beta \ \mathrm{grad}\ \tau \ \text{in}\ \Omega_R\}.$$

Here

$$\|\underset{\sim}{\boldsymbol{\sigma}}\|_{L^2,\Omega_R} \overset{\mathrm{def}}{=} \sqrt{(\underset{\sim}{\boldsymbol{\sigma}}, \underset{\sim}{\boldsymbol{\sigma}})_{L^2,\Omega_R}},$$

where

$$(\underset{\sim}{\boldsymbol{\sigma}}, \underset{\sim}{\boldsymbol{\sigma}}_1)_{L^2,\Omega_R} \equiv \int\int_{\Omega_R} \underset{\sim}{\boldsymbol{\sigma}} : \underset{\sim}{\boldsymbol{\sigma}}_1 \, \mathrm{d}\Omega \overset{\mathrm{def}}{=} \int\int_{\Omega_R} \sum_i \sum_j (\sigma)_{ij}(\sigma_1)_{ij} \, \mathrm{d}\Omega .$$

The statically admissible space for cases when non-homogeneous traction boundary conditions are prescribed, $[n]\underset{\sim}{\boldsymbol{\sigma}} = \boldsymbol{t}$, on the boundary Γ_1 and/or Γ_2 is defined by

$$\tilde{\underset{\sim}{\boldsymbol{\Sigma}}}(\Omega_R) = \{\underset{\sim}{\boldsymbol{\sigma}} \mid \underset{\sim}{\boldsymbol{\sigma}} \in \underset{\sim}{\boldsymbol{\Sigma}}(\Omega_R); \ [n]\underset{\sim}{\boldsymbol{\sigma}} = \boldsymbol{t} \ \text{on}\ \Gamma_1 \ \text{and/or}\ \Gamma_2\}.$$

One may notice that $\underset{\sim}{\boldsymbol{\Sigma}}$ and $\tilde{\underset{\sim}{\boldsymbol{\Sigma}}}$ are not linear spaces. We also define the linear space $\underset{\sim}{\boldsymbol{\Sigma}}^H(\Omega_R)$ by

$$\underset{\sim}{\boldsymbol{\Sigma}}^H(\Omega_R) = \{\underset{\sim}{\boldsymbol{\sigma}} \mid \|\underset{\sim}{\boldsymbol{\sigma}}\|_{L^2,\Omega_R} < \infty; \ \mathbf{div}\ \underset{\sim}{\boldsymbol{\sigma}} = 0 \ \text{in}\ \Omega_R\}.$$

When $[n]\underset{\sim}{\boldsymbol{\sigma}} = \mathbf{0}$ on Γ_1 and/or Γ_2 we define the space $\overset{\circ}{\underset{\sim}{\boldsymbol{\Sigma}}}{}^H(\Omega_R)$ by

$$\overset{\circ}{\underset{\sim}{\boldsymbol{\Sigma}}}{}^H(\Omega_R) = \{\underset{\sim}{\boldsymbol{\sigma}} \mid \underset{\sim}{\boldsymbol{\sigma}} \in \underset{\sim}{\boldsymbol{\Sigma}}^H(\Omega_R); \ [n]\underset{\sim}{\boldsymbol{\sigma}} = \mathbf{0} \ \text{on}\ \Gamma_1 \ \text{and/or}\ \Gamma_2\}.$$

Any finite dimensional subspaces of the above will be denoted by a subscript N, for example $\underset{\sim}{\boldsymbol{\Sigma}}{}^H_N$ is a subspace of $\underset{\sim}{\boldsymbol{\Sigma}}^H$ with $\dim \underset{\sim}{\boldsymbol{\Sigma}}{}^H_N = N < \infty$.

The dual (complementary) weak formulation for the (thermo-) elasticity problem over the sub-domain Ω_R is (see [17, pp. 103–108])

Seek $\boldsymbol{\sigma} \in \tilde{\underset{\sim}{\boldsymbol{\Sigma}}}(\Omega_R)$ such that

$$\mathscr{B}_c(\boldsymbol{\sigma}, \boldsymbol{\sigma}_1) = \mathscr{F}_c(\boldsymbol{\sigma}_1) \quad \forall\, \boldsymbol{\sigma}_1 \in \overset{\circ}{\underset{\sim}{\boldsymbol{\Sigma}}}{}^H(\Omega_R) \tag{18}$$

where

$$\mathscr{B}_c(\boldsymbol{\sigma}, \boldsymbol{\sigma}_1) = \int\int_{\Omega_R} \boldsymbol{\sigma}^{\mathrm{T}}[C]\boldsymbol{\sigma}_1 \, \mathrm{d}\Omega , \tag{19}$$

$$\mathscr{F}_c(\boldsymbol{\sigma}_1) = \int_{(\partial\Omega_R)_u} \boldsymbol{u}^{\mathrm{T}} \cdot ([n]\boldsymbol{\sigma}_1) \, \mathrm{d}s . \tag{20}$$

Here, $(\partial\Omega_R)_u$ denotes the part of the boundary where displacement boundary conditions $\boldsymbol{u}$ are prescribed.

Any statically admissible stress vector $\boldsymbol{\sigma} \in \tilde{\underset{\sim}{\boldsymbol{\Sigma}}}(\Omega_R)$ can be written as an *arbitrary known function* from $\tilde{\underset{\sim}{\boldsymbol{\Sigma}}}(\Omega_R)$ and a suitably chosen function from $\overset{\circ}{\underset{\sim}{\boldsymbol{\Sigma}}}{}^H(\Omega_R)$. Therefore, we can write

$$\boldsymbol{\sigma} = \boldsymbol{\sigma}_{\mathrm{H}} + \boldsymbol{\sigma}_{\mathrm{P}} + \overline{\boldsymbol{\sigma}}_{\mathrm{P}}$$
$$\boldsymbol{\sigma}_{\mathrm{H}} \in \boldsymbol{\Sigma}^{qH}(\Omega_R), \quad (\boldsymbol{\sigma}_{\mathrm{P}} + \overline{\boldsymbol{\sigma}}_{\mathrm{P}}) \in \tilde{\boldsymbol{\Sigma}}(\Omega_R). \tag{21}$$

With these notations, the dual weak form (18) can be restated in a more convenient way of treatment

Seek $\boldsymbol{\sigma}_H \in \boldsymbol{\Sigma}^{qH}(\Omega_R)$ such that
$\mathscr{B}_c(\boldsymbol{\sigma}_{\mathrm{H}}, \boldsymbol{\sigma}_1) = \mathscr{F}_c(\boldsymbol{\sigma}_1) - \mathscr{B}_c(\boldsymbol{\sigma}_{\mathrm{P}}, \boldsymbol{\sigma}_1) - \mathscr{B}_c(\overline{\boldsymbol{\sigma}}_{\mathrm{P}}, \boldsymbol{\sigma}_1) \quad \forall\, \boldsymbol{\sigma}_1 \in \boldsymbol{\Sigma}^{qH}(\Omega_R)$. (22)

3.1. The extraction post-solution scheme

For elastic problems without thermal loading or body forces and with homogeneous boundary conditions on $\Gamma_1 \cup \Gamma_2$, one obtains the weak form (22) without the two last terms in the right-hand side. Computation of GSIFs for this case has been addressed in detail in [9,10]. First attempt to use the methods in [9,10] for thermo-elastic problems, using the above dual weak formulation without considering the particular stress tensors is provided in [11]. *The first one or two A_is, associated with eigenvalues that are smaller than 1, i.e. stresses become infinity at $r = 0$, will be denoted by TGSIFs or TSIFs.* Mathematical analysis proved that the TSIFs can be obtained at the limit when the radius of the sub-domain Ω_R approaches zero. However, the error introduced in the extracted TSIFs at a given finite R, due to neglecting $\boldsymbol{\sigma}_{\mathrm{P}}$ and $\overline{\boldsymbol{\sigma}}_{\mathrm{P}}$ was not properly investigated. Numerical experiments for crack-tip singularities and a singular point associated with an inclusion problem involving two dissimilar materials were presented to demonstrate that indeed at very small radii R, one usually obtains good approximations of the TSIFs. From the numerical point of view this required a considerably refined mesh (with elements of an order of magnitude up to $\mathscr{O}(10^{-5})$) in the vicinity of the singular point. It has also been shown that for weak stress singularities even a very refined mesh did not provide satisfactory results.

Explicit computation of $\boldsymbol{\sigma}_{\mathrm{P}}$ and $\overline{\boldsymbol{\sigma}}_{\mathrm{P}}$ is a complicated and tedious task. Thus, we propose herein a procedure such that the TSIFs could be extracted using only the knowledge of their functional representation in r direction, and a detailed analysis of the error introduced because of neglecting them. An analysis of the error induced by not considering the particular solution provides the means to extrapolate to the limit $R = 0$ and obtain excellent results without the need for considerable mesh refinements. The model problem for the mathematical analysis will be a domain containing a reentrant corner in isotropic materials. Although this does not fully represent anisotropic materials, and multi-material interfaces, it still provides the necessary steps in the proof which can be reconstructed in a more general case.

3.2. The compliance matrix, load vector and extraction of TSIFs

The stress vectors $\boldsymbol{\sigma}_{\mathrm{H}}$, $\boldsymbol{\sigma}_1$ in (22), being in the space $\boldsymbol{\Sigma}^{qH}$, can be represented by (9), and the elements of the compliance matrix corresponding to $\mathscr{B}_c(\boldsymbol{\sigma}_{\mathrm{H}}, \boldsymbol{\sigma}_1)$ are

$$(B_c)_{ij} = \frac{R^{\alpha_i+\alpha_j}}{\alpha_i+\alpha_j} \int_0^{\omega} \boldsymbol{F}_i^{\mathrm{T}}(\theta)[C]\boldsymbol{F}_j(\theta)\,\mathrm{d}\theta, \tag{23}$$

where R is the radius of the circular sector Ω_R. For isotropic materials, the eigen-stress vectors $\boldsymbol{F}_i(\theta)$ and $\boldsymbol{F}_j(\theta)$ are orthogonal in respect to the integral in (23) (see e.g. [13, Chap. 12.2.2]), thus the compliance matrix is diagonal

$$(B_c)_{ij} = \begin{cases} \dfrac{R^{2\alpha_i}}{2\alpha_i} D_i & i = j \\ 0 & i \neq j \end{cases} \quad i, j = 1, 2, \ldots, N \tag{24}$$

and D_i are constants which depend on the angle ω, the compliance matrix $[C]$ and the eigen-stresses, but independent of R.

The load vector corresponding to the linear form $\mathscr{F}_c$ is to be evaluated only along the circular boundary Γ_R. This is because $\boldsymbol{\sigma}_1 \in \boldsymbol{\Sigma}^{qH}$, therefore $\boldsymbol{\sigma}_1 = \mathbf{0}$ at $\theta = 0, \omega$ if traction free boundary conditions are considered. The displacements vector $\boldsymbol{u}$ as $r \to 0$ is given by (10) and (17)

$$\boldsymbol{u} = \sum_{i=1}^{\infty} A_i r^{\alpha_i} \boldsymbol{f}_i(\theta) + \boldsymbol{u}_o + r\boldsymbol{g}(\theta) + \mathcal{O}(r^{\beta_1 - 1 - \epsilon}) . \tag{25}$$

To obtain the jth component of the load vector, one has to substitute (20), and the jth eigen-stress in the series (9) ($r^{\alpha_j - 1}\boldsymbol{F}_j(\theta)$) in the expression for the linear form (20). Since the homogeneous eigen-stresses are orthogonal in respect to the integral along Γ_R for isotropic materials, one obtains

$$(F_c)_j = C_{1,j} R^{\alpha_1 + \alpha_j} + C_{3,j} R^{\alpha_j - 1} + C_{4,j} R^{\alpha_j + \beta_1 + 1} + \text{h.o.t.} \quad j = 1, 2, \ldots, N . \tag{26}$$

Here, $C_{i,j}$ are constants independent of R that may be zero and depend on material properties, geometry, far field loading and temperature field.

Evaluation of the other two terms in the load vector, corresponding to $\mathscr{B}_c(\boldsymbol{\sigma}_p, \boldsymbol{\sigma}_1)$ and $\mathscr{B}_c(\overline{\boldsymbol{\sigma}}_p, \boldsymbol{\sigma}_1)$, denoted by $\mathscr{B}_{c1}$ and $\mathscr{B}_{c2}$ correspondingly, is now considered. Substituting (15) in (19), and having $\boldsymbol{\sigma}_1 \in \boldsymbol{\Sigma}^{qH}$, one obtains the jth element of the load vector corresponding to $\mathscr{B}_{c1}$

$$\begin{aligned}(\mathscr{B}_{c1})_j &= R^{\alpha_j + 1} \int_0^{\omega} \boldsymbol{\sigma}_o^{\mathrm{T}}[C]\boldsymbol{F}_j(\theta)\,\mathrm{d}\theta + R^{\alpha_j + \beta_1 + 1} \int_0^{\omega} \boldsymbol{H}^{\mathrm{T}}(\theta)[C]\boldsymbol{F}_j(\theta)\,\mathrm{d}\theta + \text{h.o.t.} \\ &= C_{5,j} R^{\alpha_j + 1} + C_{6,j} R^{\alpha_j + \beta_1 + 1} + \text{h.o.t.} \quad j = 1, 2, \ldots, N . \end{aligned} \tag{27}$$

The load vector corresponding to $\mathscr{B}_{c2}$ is very similar to that given in (27), without the first term, and we may add them together resulting with

$$(\mathscr{B}_{c1})_j + (\mathscr{B}_{c2})_j = C_{5,j} R^{\alpha_j + 1} + C_{7,j} R^{\alpha_j + \beta_1 + 1} + \text{h.o.t.} \quad j = 1, 2, \ldots, N . \tag{28}$$

In view of (24), (26) and (28), the TSIF A_1, for example, can be computed

$$\begin{aligned} A_1 &= \frac{2\alpha_1}{D_1} R^{-2\alpha_1} [C_{1,1} R^{2\alpha_1} + C_{3,1} R^{\alpha_1 - 1} + C_{4,1} R^{\alpha_1 + \beta_1 + 1} + C_{5,1} R^{\alpha_1 - 1} + C_{7,1} R^{\alpha_1 + \beta_1 + 1} + \text{h.o.t.}] \\ &= \frac{2\alpha_1}{D_1} [C_{1,1} + C_{8,1} R^{1 - \alpha_1} + C_{4,1} R^{1 + \beta_1 - \alpha_1} + \text{h.o.t.}] \end{aligned} \tag{29}$$

Examining (29) as $R \to 0$, one notices that the influence of the particular stress vector on A_1 is of an order of magnitude of $R^{1-\alpha_1}$ or $R^{1+\beta_1-\alpha_1}$ (depending on whether $C_{8,1}$ is zero or not). The stress field in the neighborhood of a singular point is singular only if $\alpha_1 < 1$, and because $\beta_1 \geq 0$, the influence approaches zero as $R \to 0$. This suggests that the terms associated with the particular stress vectors could be neglected, contributing to a relative error of an order of magnitude $\mathcal{O}(R^{1-\alpha_1})$ or $\mathcal{O}(R^{1+\beta_1-\alpha_1})$ when computing A_1, for example. Using a finite sub-domain of radius R_1, $(A_1)_1$ can be extracted by (29) neglecting the particular stress vector (only the first term in the right-hand side considered). By repeating this extraction procedure over a sequence of decreasing sub-domains of radii $R_j, R_j < R_{j-1} < \cdots < R_1$, one obtains a sequence of approximations denoted by $(A_1)_j$. Then, employing Richardson extrapolation [18, pp. 94–95] with the error behaving as $R^{1-\alpha_1}$ or $R^{1+\beta_1-\alpha}$, A_1 can be extrapolated at the limit $R \to 0$. We can generate a table of A_1s, for example, by the recursive formula

$$(A_1)_j^{(m)} = (A_1)_{j-1}^{(m+1)} + \frac{(A_1)_{j-1}^{m+1} - (A_1)_{j-1}^{(m)}}{(R_j/R_{j+m})^{\gamma} - 1} \tag{30}$$

where γ is either $1 - \alpha_1$ or $1 + \beta_1 - \alpha_1$, and the accuracy of A_1 improves as j and m increase (j corresponds to the radius R_j of the sub-domains Ω_R which is the row number in the generated table, and m corresponds to the column number—see Table 2 for example).

REMARK 1. If A_2 is to be computed, for example, the same procedure holds with γ either $1 - \alpha_2$ or $1 + \beta_1 - \alpha_2$ in (30).

REMARK 2. The situation described in (16) will affect the third term in (29), and it seems as the leading term may sometimes be of an order of $R^{1+\beta_1-\alpha_1}|1 + \ln(R)|$. However, this is not the case, and this will be demonstrated by numerical examples on cracked domains, where the temperature field is proportional to $r^{1/2}$ and the homogeneous stress field is proportional to $r^{-1/2}$.

REMARK 3. For anisotropic materials, or multi-material interfaces, the compliance matrix $[B_c]$ is fully populated, and an explicit equation as (29) is not obtainable. However, computation of the TGSIFs neglecting the particular stress tensor, for several R_js and extrapolating to the limit is still valid due to similar arguments (this will be shown by a numerical example). The mathematical analysis of this case is more cumbersome and is not provided herein.

3.3. Discretization and the numerical algorithm

For solving (22), the displacements along $(\partial\Omega_R)_u$ are to be substituted in (20). These are assumed for the mathematical analysis to be known, but in the numerical realization we substitute in (22) the displacements extracted from a finite element solution. Instead of $\boldsymbol{u}_{\mathrm{EX}}$ we obtain an approximation $\boldsymbol{u}_{\mathrm{FE}}$ by the 'classical' finite element method (FEM) based on the principle of virtual work. Of course, $\boldsymbol{u}_{\mathrm{FE}}$ approximates the thermo-elastic displacements field, with thermal loading being imposed on the domain of interest, and its accuracy can be controlled by p- or hp-extensions (see e.g. [13]). The proposed procedure is a post-solution operation performed after the thermo-elastic problem over entire domain (Ω) is solved by the FEM, and having obtained $\boldsymbol{u}_{\mathrm{FE}}$.

The weak form (22) is further discretized by choosing a statically admissible subspace $\boldsymbol{\Sigma}_N^{sH}(\Omega_R)$ constructed as a linear combination of the first N eigen-pairs according to (9), with A_i^{FE}, $i = 1, 2, \ldots, N$ being sought. In general, also the eigen-pairs are not known explicitly and are computed by the modified Steklov method [9]. Thus, the algorithm for computing TGSIFs is the following:

(a) Compute the smallest eigenvalue β_1 associated with the flux singularity (by the modified Steklov method) and the corresponding generalized flux intensity factor $(\mathrm{GFIF})_1$. If $(\mathrm{GFIF})_1 = 0$, use as β_1 the next smallest eigenvalue, i.e. β_2.

(b) Obtain a finite element solution of the thermal problem, then impose it as a thermal loading and solve the elasticity problem to obtain the displacements finite element solution $\boldsymbol{u}_{\mathrm{FE}}$. Both the thermal and the elasticity solutions should have a small relative error measured in the energy norm.

(c) Extract TGSIFs by the principle of minimum complementary energy for *several values of integration radii* R_i. The radius of integration R_i should always be outside the first layer of elements which have a vertex in the singular point. At each integration radius R_i, the TGSIFs should be extracted using the finite element solutions corresponding to $p = 1, 2, \ldots, 8$, and estimated for $p \to \infty$. This ensures that discretization errors associated with replacing $\boldsymbol{u}_{\mathrm{EX}}$ by $\boldsymbol{u}_{\mathrm{FE}}$ are small.

(d) Use Richardson extrapolation with the error behaving as either $R^{\beta_1 - 1 - \alpha_1}$ or $R^{1-\alpha_1}$ to determine the first stress intensity factor and $R^{\beta_1 - 1 - \alpha_2}$ or $R^{1-\alpha_2}$ to determine the second, as $R \to 0$.

(e) Examine the columns in the table generated by Richardson extrapolation and ensure that the elements in the columns have similar values. Also, examine the Richardson extrapolation table for $p \to \infty$ in comparison with the table for $p = 8$ and ensure the values are close (see following example problems).

(f) Redo step (c), with a larger statically admissible space, i.e. increased number of homogeneous eigen-stresses N, then redo steps (d)–(e). Examine that the obtained TGSIFs are virtually independent of N. This reassures the reliability of the results.

In all examples, the integration is performed along a circle of radius R greater than the radius of the elements having a vertex at the singular point. This is because the finite element solution in the first group of elements at the singular point is not of high accuracy. Numerical examples are presented in the following to demonstrate that the proposed method performs well, resulting in accurate TGSIFs.

4. Numerical examples of crack tip singularities

The following problems are solved by means of a p-version finite element computer code, called STRESS CHECK[1]. The temperature distribution is computed by solving the steady-state heat conduction problem which is thereafter imposed as a thermal load in the elastostatic analysis. The trial space used in the finite element analysis was the trunk space [13, Chap. 6].

[1] STRESS CHECK is a trademark of Engineering Software Research and Development, Inc. 7750 Clayton Road, Suite 204, St. Louis, MO 63117.

4.1. Central crack in a rectangular plate

A rectangular plate with a central crack subjected to two different thermal loadings, for which numerical results are reported in previous publications is considered. Analytical (exact) solutions to practical problems are very difficult, if not impossible to obtain, and to the best of the author's knowledge no analytic solutions are available to finite geometry models. The rectangular plate of width $2W$ and length $2L$ and a central crack of length $2a = 2$ with $L/W = 1.0$ and $a/W = 0.2$ is solved for two different sets of thermal loadings representing pure mode I and pure mode II (see Fig. 2).

The heat conduction coefficients are taken to be $a_{11} = a_{22} = 1$, $a_{12} = 0$, (results are independent of the heat conductivity for isotropic materials) and the mechanical material properties are: Young's modulus $E = 1$; Poisson's ratio $\nu = 0.3$; and the coefficient of linear thermal expansion $\alpha = 0.01$. Plane strain condition is assumed. Taking advantage of the symmetry of the problem, only half of the model has been solved, imposing the following symmetry boundary conditions at $|y| \leq L$, $x = 0$: $q_n = \partial\tau/\partial x = 0$, $u_x = 0$. The finite element mesh surrounding the crack tip contains *only one layer* graded in a geometric progression in the vicinity of the singular point with the grading factor 0.15. Fig. 3 shows the finite element mesh used in our computation. The results are compared with these previously published in [4,5,11,19–21]. Sumi et al. [4] extracted the TSIFs using the modified-collocation and complex variable methods. Prasad et al. [19] reported the TSIFs obtained by employing the boundary element method (BEM), simultaneously solving the thermal and elasticity problem, then extracting the TSIFs using the path-independent J-integral. Lee et al. [20] used the BEM, first solving the thermal problem, then the elastic problem and finally computing the TSIFs by the displacement extrapolation method. Tsai et al. [5] solved the mode I problem using the thermal weight function and the h-version finite

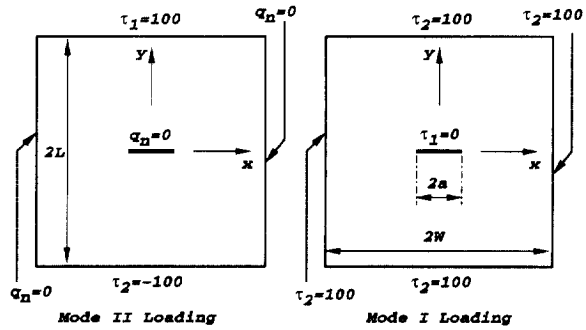

Fig. 2. Geometry and boundary conditions of a rectangular plate with a central crack.

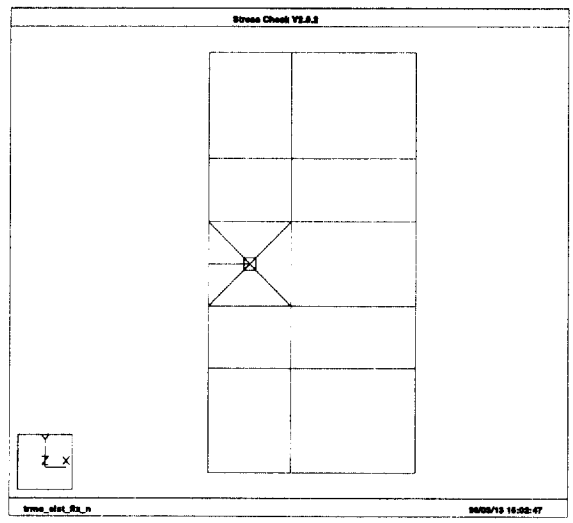

Fig. 3. The finite element mesh for the rectangular plate with a central crack.

element method. Liu et al. [21] used the BEM, coupling the direct boundary integral equations to crack integral equations, to extract the mode II TSIF. Yosibash showed in [11] that the TIFs can be obtained by the complementary energy principle in a limit process as $R \to 0$. The method presented in [11] requires a very fine mesh in the neighborhood of singular points, resulting in many layers with very small radii $\mathcal{O}(R) = 0.0006$, thus it is inefficient. Herein, these TSIFs are extracted at large Rs using same procedure described in [11], then using Richardson extrapolation.

Mode I thermal loading

The quality of the finite element solution is summarized in Table 1. Examining the first eigenvalue of the thermal singularity, and the first two eigenvalues of the elasticity problem one observes that

$$\beta_1 + 1 - \alpha_1 = 1/2 + 1 - 1/2 = 1 \tag{31}$$

$$\beta_1 + 1 - \alpha_2 = 1/2 + 1 - 1/2 = 1 \tag{32}$$

Extracted values of $(K_I)_{FE}$ at $p = 8$ and as $p \to \infty$ for different values of R are listed in Tables 2 and 3, respectively, together with the Richardson extrapolated values as $R \to 0$. $(K_{II})_{FE}$ is 0.000000000 for all cases. By the mathematical analysis, the error in $(K_I)_{FE}$ and $(K_{II})_{FE}$ behaves like R^1 as $R \to 0$. This power is used for Richardson extrapolation. Extraction of $(K_I)_{FE}$ at the smallest integration radius $R = 0.3$ is the least accurate because the integration path is the closest to the first layer of elements surrounding the singular point, therefore

Table 1
Convergence of the FE solution for mode I loading—center crack

p-level	Thermal analysis		Elasticity analysis	
	DOF	Estimated $\|e\|_{E(\Omega)}$ (%)	DOF	Estimated $\|e\|_{E(\Omega)}$ (%)
1	12	30.55	45	73.23
2	44	12.31	129	18.81
3	81	8.15	223	10.28
4	137	5.61	355	6.42
5	212	4.43	525	4.50
6	306	3.69	733	3.53
7	419	3.18	979	2.89
8	551	2.80	1263	2.42

Table 2
$(K_I)_{FE}$ at various values of R, $p = 8$, for mode I center crack problem and the extrapolated values as $R \to 0$

R	$(K_I)_{FE} \overset{def}{=} K_I^{(0)}$	$K_I^{(1)}$	$K_I^{(2)}$	$K_I^{(3)}$
0.9	1.7506058183	0.8192715659	0.8001684752	0.7882428331
0.7	1.5436426511	0.8107813034	0.7922180471	
0.5	1.3342536946	0.8001737284		
0.3	1.1206217081			

Table 3
$(K_I)_{FE}$ at various values of R, $p \to \infty$, for mode I center crack problem and the extrapolated values as $R \to 0$

R	$(K_I)_{FE} \overset{def}{=} K_I^{(0)}$	$K_I^{(1)}$	$K_I^{(2)}$
0.9	1.7522014811	0.8243398522	0.7997843595
0.7	1.5460100080	0.8134262999	
0.5	1.3367003771		

The value of $R = 0.3$ was not considered because it was away from the value obtained at $p = 8$, therefore the extrapolated value is not accurate enough.

contains the largest *numerical error*. One may gain further accuracy by adding an additional layer of elements. Numerical experiments support the last statement.

Tables 2 and 3 clearly demonstrate that the thermal stress intensity factor is extrapolated with high accuracy, even though the relative errors at finite values of R are very large. The significant reduction in the error already at the first step of the Richardson algorithm, and the similarity of the results in each column, strongly support the mathematical analysis.

The extrapolated value is in excellent agreement with [4,11,19]. A summary of results obtained by other numerical methods compared with the extrapolated K_I is given in Table 7.

Mode II thermal loading

This subsection summarizes the TSIFs obtained when the domain is loaded by mode II thermal loading. The quality of the finite element solution is summarized in Table 4. Extracted values of $(K_{II})_{FE}$ at $p = 8$ and as $p \to \infty$ for different values of R are listed in Tables 5 and 6, respectively, together with the Richardson extrapolated values as $R \to 0$. $(K_I)_{FE}$ is 0.000000000 for all cases. Again, the error in $(K_{II})_{FE}$ behaves like R^1 as $R \to 0$. This power is used for Richardson extrapolation. Tables 5 and 6 present a picture very similar to that of the corresponding Tables 2 and 3 of the previous mode I problem. Again, one may notice the convergence achieved by the extrapolation algorithm, although the TSIFs at the various Rs are of very low accuracy. The very similar values in Tables 5 and 6 demonstrate that the numerical error in $(K_{II})_{FE}$ is small at the given radii, thus high confidence in the extrapolated results is achieved.

In Table 7 we summarize the results obtained, compared to those reported previously for the mode I and mode II loadings. The results obtained herein show a good accuracy compared with those reported previously.

Table 4
Convergence of the FE solution for mode II loading—center crack

p-level	Thermal analysis		Elasticity analysis	
	DOF	Estimated $\|e\|_{E(\Omega)}$ (%)	DOF	Estimated $\|e\|_{E(\Omega)}$ (%)
1	21	8.98	45	669.68
2	62	4.44	129	35.11
3	108	2.72	223	30.03
4	173	2.02	355	7.72
5	257	1.58	525	5.65
6	360	1.32	733	4.39
7	482	1.13	979	3.66
8	623	0.99	1263	3.13

Table 5
$(K_I)_{FE}$ at various values of R, $p = 8$, for mode II center crack problem and the extrapolated values as $R \to 0$

R	$(K_{II})_{FE} \overset{\text{def}}{=} K_{II}^{(0)}$	$K_{II}^{(1)}$	$K_{II}^{(2)}$	$K_{II}^{(3)}$
0.9	−0.0693129872	0.1246962094	0.1219032328	0.1212235415
0.7	−0.0261998324	0.1234548865	0.1214501053	
0.5	0.0165586587	0.1223092972		
0.3	0.0588589141			

Table 6
$(K_{II})_{FE}$ at various values of R, $p \to \infty$, for mode II center crack problem and the extrapolated values as $R \to 0$

R	$(K_{II})_{FE} \overset{\text{def}}{=} K_{II}^{(0)}$	$K_{II}^{(1)}$	$K_{II}^{(2)}$	$K_{II}^{(3)}$
0.9	−0.0693143367	0.1248325230	0.1229332211	0.1210350940
0.7	−0.0261705901	0.1239883888	0.1216678030	
0.5	0.0167319753	0.1226623398		
0.3	0.0591041211			

Table 7
Summary of mode I and mode II TSIFs

Ref. Meth.	Tsai et al. [5] Weight fncn & FEM	Lee et al. [20] BEM	Prasad et al. [19] BEM	Sumi et al. [4] Complex var. & collocation	Liu et al. [21] BEM	Yosibash [11] Compl. Enrg. w/o Rich. Ext.	Present method
K_{I}	0.8036	0.8593	0.7759	0.7759		0.7784	0.7998
K_{II}		0.1317	0.1207	0.1185	0.1324	0.1214	0.1210

The number of degrees of freedom in the FE model is half of those needed in [11] for obtaining similar accuracy in the TSIFs.

4.2. Slant crack in a rectangular plate

A rectangular plate with a central crack slanted at an angle 60° to the x-axis is considered. The geometry and temperature boundary conditions are shown in Fig. 4. The rectangular plate of width $2W=2$ with $L/W=2.0$ and $a/W=0.3$ is solved for a temperature loading which gives rise to mixed mode. The heat conduction coefficients are taken to be $a_{11}=a_{22}=1$, $a_{12}=0$, and the mechanical material properties are: Young's modulus $E=2.184\times10^{5}$; Poisson's ratio $\nu=0.3$; and the coefficient of linear thermal expansion $\alpha=1.67\times10^{-5}$. Plane stress condition is assumed.

The results are compared with those obtained by Nakanishi et al. [22] by the complex variable method, and reported in [23, pp. 1063–1067]. The finite element mesh surrounding the crack tip contains several layers graded in a geometric progression in the vicinity of the singular point with the grading factor 0.15. The finite element mesh is presented in Fig. 5. The finite element discretization error in energy norm at $p=8$ (1834 dof) for the thermal analysis is 0.18%, and for the thermo-elastic analysis (3797 dof) is 1.15%. This model problem is used to demonstrate that the number of terms used to represent $\tilde{\Sigma}^{sH}$ has minor influence on the extracted TSIFs. Also, we show that Richardson extrapolation for K_{I} assumes that the error is $\mathcal{O}(R^{1-\alpha_1})$ wheres for K_{II} is $\mathcal{O}(R^{1+\beta_1-\alpha_2})$. For the slant crack configuration $\alpha_1=\alpha_2=\beta_1=1/2$, thus γ in (30) is either $1/2$ or 1. Extracted values of $(K_{\mathrm{I}})_{\mathrm{FE}}$ at $p\to\infty$ for different values of R are listed in Table 8 when $N=2,4,6$ with $\gamma=1/2$, and in Table 9 with $\gamma=1$, together with the Richardson extrapolated values as $R\to0$. This is to demonstrate that the error in $(K_{\mathrm{I}})_{\mathrm{FE}}$ behaves like $R^{1/2}$ as $R\to0$. Table 9 demonstrates that the coefficient $C_8\neq0$ in (29) for K_{I},

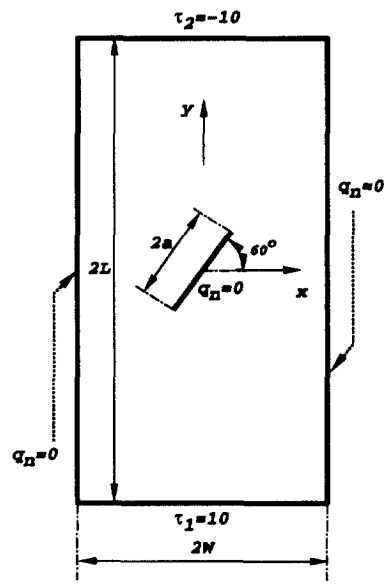

Fig. 4. Geometry and boundary conditions of a rectangular plate with a slanted crack.

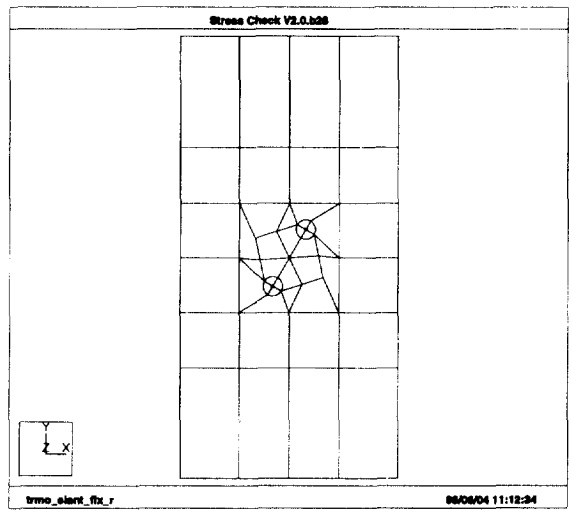

Fig. 5. The finite element mesh for the rectangular plate with a slant crack.

Table 8
$(K_I)_{FE}$ at various values of R, at $p \to \infty$ taking $\gamma = 1/2$ for a plate with a slant crack with $N = 2, 4, 6$, and extrapolated values as $R \to 0$

R	$(K_I)_{FE} \overset{def}{=} K_I^{(0)}$			$K_I^{(1)}$			$K_I^{(2)}$			$K_I^{(3)}$			$K_I^{(4)}$		
	$N=2$	$N=4$	$N=6$	$N=2$	$N=4$	$N=6$	$N=2$	$N=4$	$N=6$	$N=2$	$N=4$	$N=6$	$N=2$	$N=4$	$N=6$
0.085	−2.995	−2.536	−1.962	0.2071	0.2222	0.0261	−0.0305	−0.0345	0.0230	0.0236	0.0236	0.0236	0.02381	0.02388	0.02342
0.04	−1.990	−1.670	−1.338	0.0847	0.0900	0.0246	0.0051	0.0037	0.0234	0.0237	0.0238	0.0235			
0.02	−1.382	−1.154	−0.939	0.0449	0.0468	0.0240	0.0171	0.0167	0.0235						
0.01	−0.964	−0.802	−0.657	0.0310	0.0318	0.0237									
0.005	−0.673	−0.624	−0.457												

Table 9
$(K_I)_{FE}$ at various values of R, at $p \to \infty$ taking $\gamma = 1$ for a plate with a slant crack with $N = 2, 4, 6$, and extrapolated values as $R \to 0$

R	$(K_I)_{FE} \overset{def}{=} K_I^{(0)}$			$K_I^{(1)}$			$K_I^{(2)}$			$K_I^{(3)}$			$K_I^{(4)}$		
	$N=2$	$N=4$	$N=6$	$N=2$	$N=4$	$N=6$	$N=2$	$N=4$	$N=6$	$N=2$	$N=4$	$N=6$	$N=2$	$N=4$	$N=6$
0.085	−2.995	−2.536	−1.962	−1.09	−0.90	−0.78	−0.676	−0.558	−0.465	−0.443	−0.365	−0.300	−0.297	−0.243	−0.199
0.04	−1.990	−1.670	−1.338	−0.77	−0.64	−0.54	−0.470	−0.388	−0.320	−0.310	−0.251	−0.205			
0.02	−1.382	−1.154	−0.939	−0.55	−0.45	−0.37	−0.326	−0.268	−0.258						
0.01	−0.964	−0.802	−0.657	−0.38	−0.32	−0.26									
0.005	−0.673	−0.624	−0.457												

Table 10
$(K_{II})_{FE}$ at various values of R, at $p \to \infty$ for a plate with a slant crack with $N = 2, 4, 6$, and extrapolated values as $R \to 0$

R	$(K_{II})_{FE} \overset{def}{=} K_{II}^{(0)}$			$K_{II}^{(1)}$			$K_{II}^{(2)}$			$K_{II}^{(3)}$			$K_{II}^{(4)}$		
	$N=2$	$N=4$	$N=6$	$N=2$	$N=4$	$N=6$	$N=2$	$N=4$	$N=6$	$N=2$	$N=4$	$N=6$	$N=2$	$N=4$	$N=6$
0.085	−0.3183	−0.3183	−0.3452	−0.6445	−0.6445	−0.6440	−0.6418	−0.6418	−0.6417	−0.6461	−0.6460	−0.6457	−0.6422	−0.6422	−0.6423
0.04	−0.4909	−0.4909	−0.5034	−0.6424	−0.6424	−0.6422	−0.6455	−0.6455	−0.6452	−0.6424	−0.6424	−0.6425			
0.02	−0.5667	−0.5667	−0.5728	−0.6448	−0.6448	−0.6445	−0.6428	−0.6428	−0.6428						
0.01	−0.6057	−0.6057	−0.6086	−0.6433	−0.6433	−0.6428									
0.005	−0.6245	−0.6245	−0.6259												

whereas, as will be shown in Table 10, $C_8 = 0$ for K_{II}. This is possible because C_8 represents an integral of the corresponding eigen-stress multiplied by the particular stress vector, and for some cases these are orthogonal. The similarity of the results along the columns in Table 8, starting at $K_I^{(3)}$, and the convergence of Richardson

extrapolation to the same value for $N = 2, 4$ and 6 reassures that accurate and reliable results are obtained. Although at finite radii of integration R_i the extracted TSIFs are extremely inaccurate, the extrapolation approximation $K_I = 0.0238, 0.0234$ *is in excellent agreement with the value* $K_I \approx 0.023$ *given in [22] in a graph.*

The value K_{II} is extrapolated at the limit $R \to 0$ with γ in (30) being 1. Extracted values of $(K_{II})_{FE}$ at $p \to \infty$ for different values of R are listed in Table 10 when $N = 2, 4, 6$ together with the Richardson extrapolated values as $R \to 0$. The values in Table 10 clearly demonstrate the convergence of K_{II} to -0.6428, -0.6433 *which is in excellent agreement with the value* -0.64 *reported in [22].*

4.3. Rectangular plate with cracks at an internal hole

A rectangular plate of width $2W$, length $2L$ with a circular hole of radius ρ and two cracks emanating from it is considered, and shown in Fig. 6. Dimensions of the analyzed problem are defined by $L/W = 1$, $a = 0.4W = 1$, and two different radii $\rho/a = 0.25$ and $\rho/a = 0.75$. The material properties are identical to those described in Subsection 4.1. This problem is analyzed for one set of thermal boundary conditions, representing mode I loading, namely, $\tau_1 = 0$ on cracks and circular hole and $\tau_2 = 100$ on the outer boundary. Due to the symmetry only half of the model has been considered, and the finite element meshes for the two different radii ρ are shown in Fig. 7. The finite element mesh surrounding the crack tip contains two layers graded in a geometric progression in the vicinity of the singular point with the grading factor 0.15. The quality of the finite element solution is summarized in Table 11. Extracted values of $(K_I)_{FE}$ at $p = 8$ and as $p \to \infty$ for different values of R

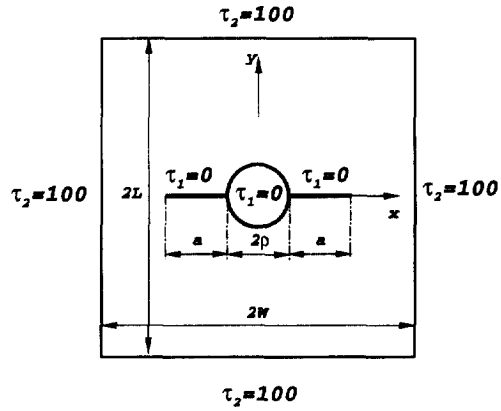

Fig. 6. Geometry and boundary conditions of a rectangular plate with a crack at an internal hole.

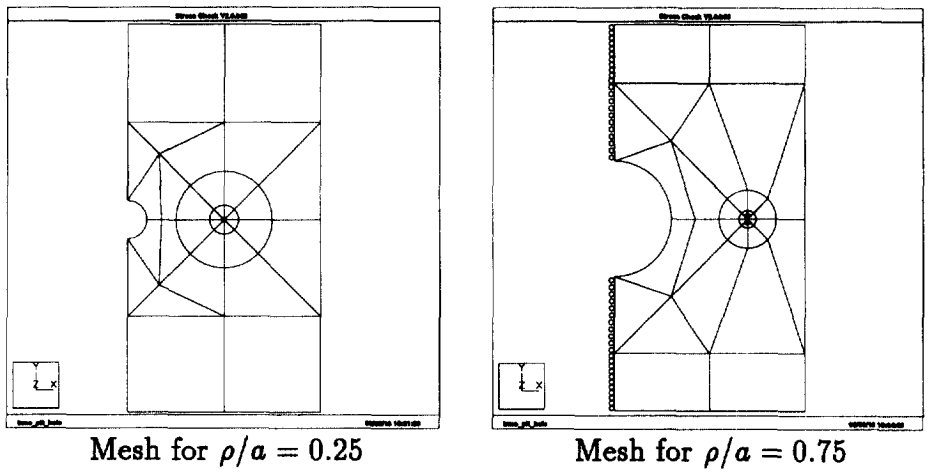

Fig. 7. Finite element meshes for the rectangular plate with a crack at an internal hole.

Table 11
Convergence of the FE solution for a plate with a crack at an internal hole

p-level	$\rho/a = 0.25$				$\rho/a = 0.75$			
	Thermal analysis		Elasticity analysis		Thermal analysis		Elasticity analysis	
	DOF	Estimated $\|e^t\|_{E(\Omega)}$ (%)	DOF	Estimated $\|e^t\|_{E(\Omega)}$ (%)	DOF	Estimated $\|e\|_{E(\Omega)}$ (%)	DOF	Estimated $\|e\|_{E(\Omega)}$ (%)
1	27	18.34	91	73.09	27	19.83	91	102.20
2	97	5.58	267	15.18	97	6.56	267	33.31
3	179	3.66	467	11.31	179	5.15	467	21.71
4	303	2.32	751	4.70	303	2.11	751	9.94
5	469	1.65	1119	3.00	469	1.28	1119	4.60
6	677	1.30	1571	2.15	677	0.95	1571	2.38
7	927	1.07	2107	1.62	927	0.76	2107	1.47
8	1219	0.90	2727	1.26	1219	0.63	2727	0.96

Table 12
$(K_I)_{FE}$ at various values of R, $p = 8$ and $p \to \infty$ (in parenthesis), for a plate with a crack at an internal hole, $\rho/a = 0.25$, and extrapolated values as $R \to 0$

R	$(K_I)_{FE} \overset{\text{def}}{=} K_I^{(0)}$	$K_I^{(1)}$	$K_I^{(2)}$	$K_I^{(3)}$
0.5	1.4822 (1.4823)			
0.3	1.2167 (1.2196)	0.8184 (0.8255)	0.8018 (0.7997)	0.7950 (0.8011)
0.1	0.9423 (0.9431)	0.8051 (0.8049)	0.7957 (0.8010)	
0.05	0.8698 (0.8724)	0.7973 (0.8016)		

Table 13
$(K_I)_{FE}$ at various values of R, $p = 8$ and $p \to \infty$ (in parenthesis), for a plate with a crack at an internal hole, $\rho/a = 0.75$, and extrapolated values as $R \to 0$

R	$(K_I)_{FE} \overset{\text{def}}{=} K_I^{(0)}$	$K_I^{(1)}$	$K_I^{(2)}$	$K_I^{(3)}$
0.35	1.4083 (1.4084)			
0.15	1.1477 (1.1483)	0.9523 (0.9532)	0.9381 (0.9428)	0.9317 (0.9342)
0.08	1.0514 (1.0535)	0.9414 (0.9452)	0.9322 (0.9349)	
0.03	0.9781 (0.9807)	0.9341 (0.9370)		

are listed in Table 12 for $\rho/a = 0.25$ and in Table 13 for $\rho/a = 0.75$ together with the Richardson extrapolated values as $R \to 0$. Again, the error in $(K_I)_{FE}$ behaves like R^1 as $R \to 0$ and this power is used for Richardson extrapolation. $(K_{II})_{FE}$ is 0.000000000 for all cases. The approximated K_I for the case $\rho/a = 0.25$ obtained by the BEM and reported in [19] is 0.806 which is in good agreement with our extrapolated value of 0.8011. For the case $\rho/a = 0.75$ we obtain $K_I = 0.9342$ which is again in good agreement with the value 0.941 reported in [19].

5. Numerical examples of singular points associated with multi-material interfaces

Composite bodies consisting of two dissimilar isotropic, homogeneous and elastic wedges, perfectly bonded along all their interfaces (or some), are studied. Two examples are provided: an inclusion problem subjected to a temperature field which exhibits singular behavior of the temperature flux, and a body consisting of two dissimilar materials subjected to a uniform elevated temperature field.

5.1. Inclusion problem

Consider the unit circle domain Ω, divided into two sectors: Ω_1 occupying the sector $-5\pi/6 \leqslant \theta \leqslant 5\pi/6$ and Ω_2 occupying the sector $5\pi/6 \leqslant \theta \leqslant 7\pi/6$, see Fig. 8. The heat conduction coefficients in Ω_1 are $a_{11} = a_{22} = 10$, $a_{12} = 0$, and in Ω_2 are $a_{11} = a_{22} = 1$, $a_{12} = 0$. Plane strain condition is assumed with $\nu_1 = \nu_2 = 0.3$, $E_1 = 10$, $E_2 = 1$, and the coefficient of linear thermal expansion is $\alpha = 0.1$ in Ω_1 and $\alpha = 0.01$ in Ω_2.

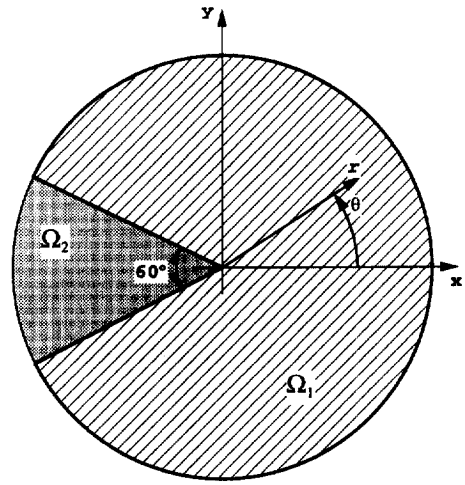

Fig. 8. Domain configuration of the inclusion problem.

The stress tensor in the domain is singular at $r = 0$, and can be written in the form

$$(\sigma_{ij}) = \frac{A_1}{\sqrt{2\pi}} r^{\alpha_1 - 1} F_{ij}^{(\mathrm{I})}(\theta) + \frac{A_2}{\sqrt{2\pi}} r^{\alpha_2 - 1} F_{ij}^{(\mathrm{II})}(\theta) - \mathcal{O}(r^{1+\epsilon}) \quad ij = r, \theta, r\theta\,, \tag{33}$$

where $F_{ij}^{(\mathrm{I})}(\theta)$ and $F_{ij}^{(\mathrm{II})}(\theta)$ are eigen-stresses given in [24]. The domain Ω is discretized by employing the finite element mesh shown in Fig. 9, having several radial layers graded geometrically toward the singular point with a grading factor 0.15. The error in energy norm for the thermal analysis at $p = 8$ (1244 dof) is less than 0.4% and in the thermo-elastic analysis (2474 dof) is less than 1.6%. Using two terms for spanning $\boldsymbol{\Sigma}^{sH}$, $N = 2$, the error in the first two TGSIFs for any given radius R converges to zero as p is increased, with a relative error at $p = 8$ which is less than 0.01%.

The temperature distribution is first computed when applying temperature boundary conditions on the boundary of Ω_1

$$\tau(\theta) = 100 \frac{(5\pi/6 - |\theta|)}{5\pi/6}, \quad -5\pi/6 \leq \theta \leq 5\pi/6\,,$$

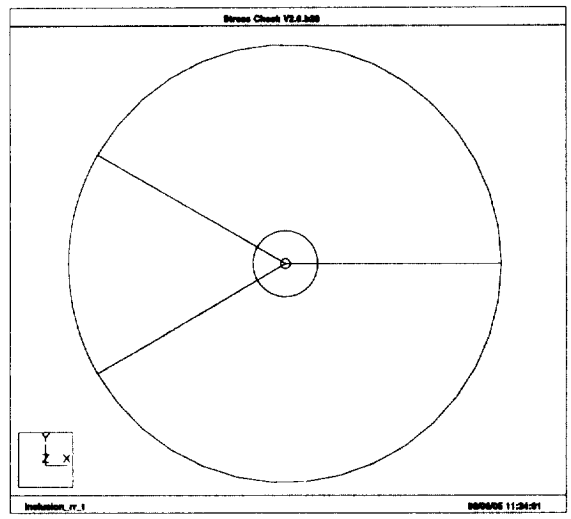

Fig. 9. Finite element mesh for inclusion problem.

and flux boundary condition on the boundary of Ω_2

$$\frac{\partial \tau}{\partial r}(\theta) = \frac{(5\pi/6-\theta)(5\pi/6+\theta)}{(5\pi/6)^2}, \quad -5\pi/6 \geq \theta \geq -\pi, 5\pi/6 \leq \theta \leq \pi .$$

The temperature distribution is then applied as a thermal load in the thermo-elastic analysis, imposing fixed boundary conditions at $r = 1$

$$\boldsymbol{u}(r=1,\theta) = \mathbf{0}, \quad 0 \leq \theta \leq 2\pi .$$

For this problem we obtain $\alpha_1 = 0.6900333$ and $\alpha_2 = 0.7940938$, and since the temperature field in the vicinity of the singular point is of the form (2), with $\tau_0 \neq 0$, we use for Richardson extrapolation the power $1-\alpha_1 = 0.3099667$ for A_1. A_2 is 0.00000000, and we report in Table 14 the normalized values of A_1 defined by: $A_1^* \overset{\text{def}}{=} -0.1040854 A_1$ obtained from the FE analysis corresponding to $p \to \infty$ and the Richardson extrapolation. Unlike in [11], where this example problem demonstrated that no convergence was visible (without extrapolation) even at a radius of $R = \mathcal{O}(10^{-5})$, herein, the proposed extrapolation methodology provides good results with integration radii which are much larger.

The examine the influence of N on the extrapolated value of A_1^* we summarize in Table 15 the extrapolated values obtained with $N = 2, 4, 6$. This again demonstrates that A_1^* is virtually independent of N.

5.2. Two 90° dissimilar bonded wedges

Two isotropic, homogeneous rectangular blocks of length $L = 10$, $L/h_1 = 10$, $L/h_2 = 5$, having different material properties are bonded together and clamped at their left boundary as shown in Fig. 10. Starting from a uniform reference temperature, the body is heated uniformly by $\Delta\tau = 100$. Due to mismatch of the coefficients of thermal expansion of the two materials, the thermo-elastic stress field is singular at point P (there are other singular points at the left boundary which are not of primary interest). Under the assumption of plane stress, a

Table 14
A_1^* at various values of R, $p \to \infty$, for inclusion problem, and the extrapolated values as $R \to 0$

R	$(A_1^*)_{FE} \overset{\text{def}}{=} (A_1^*)^{(0)}$	$(A_1^*)^{(1)}$	$(A_1^*)^{(2)}$	$(A_1^*)^{(3)}$	$(A_1^*)^{(4)}$	$(A_1^*)^{(5)}$
0.9	0.001209					
0.5	0.010198	0.055176				
0.1	0.036791	0.077903	0.101188			
0.05	0.046346	0.086209	0.094183	0.089350		
0.01	0.063177	0.089198	0.092068	0.091173	0.091774	
0.005	0.068466	0.090529	0.091807	0.091636	0.091782	0.091785

Table 15
Extrapolated A_1^* for different Ns

$N = 2$	$N = 4$	$N = 6$
0.091785	0.091510	0.091792

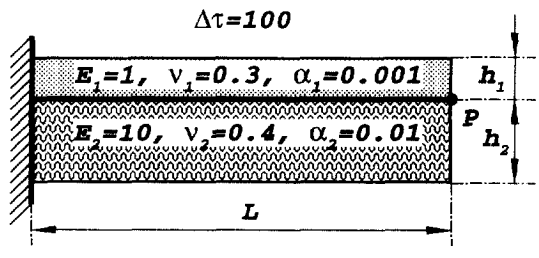

Fig. 10. Domain configurtion of 90° dissimilar bonded wedges.

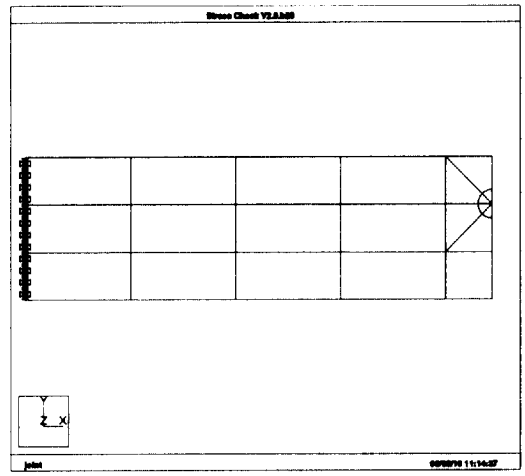

Fig. 11. Finite element mesh for 90° dissimilar bonded wedges.

thermo-elastic finite element analysis was performed, imposing a uniform temperature field over the domain. The domain is discretized by employing the finite element mesh shown in Fig. 11, having several radial layers graded geometrically toward the singular point P with a grading factor 0.15.

The eigenvalues and eigen-stresses are extracted by the modified Steklov method. Only the first eigenvalue associated with point P, $\alpha_1 = 0.8446825$ imposes a weak singularity ($\alpha_2 \geq 1$), and the x- and y-components of the homogeneous first eigen-stress vector (i.e. $(F_{11})_1(\theta)$ and $(F_{22})_1(\theta)$) are given in Fig. 12. A uniform temperature distribution over the whole domain, not being influenced by the presence of the singular point P, results in a particular stress field as presented in (14). Thus, we use for Richardson extrapolation the power $1 - \alpha_1 = 0.1553175$ for finding A_1.

In Table 16 the values A_1 obtained from the FE analysis with $N = 2$, corresponding to $p \to \infty$ and the Richardson extrapolation, are summarized. Comparing the extrapolated value of A_1 with those obtained at any finite R we notice that the value obtained even at $R = 0.01$ is off by more than 30%.

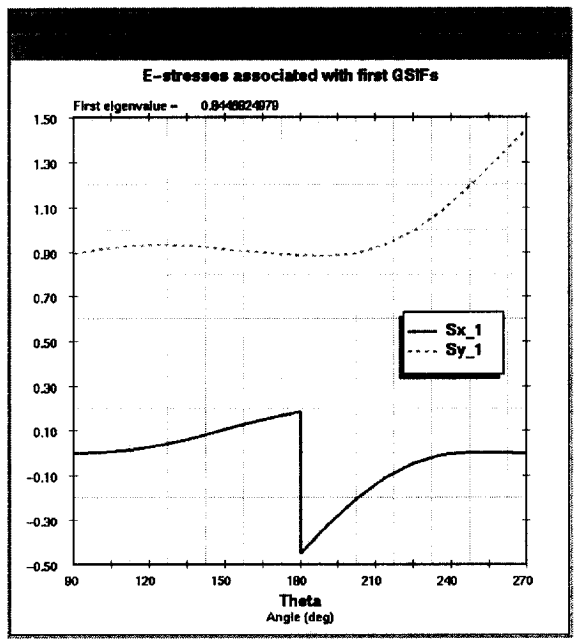

Fig. 12. $(F_{11})_1(\theta)$ and $(F_{22})_1(\theta)$ for 90° dissimilar bonded wedges.

Table 16
A_1 at various values of R, $p \to \infty$, for 90° dissimilar bonded wedges, and the extrapolated values as $R \to 0$

R	$(A_1)_{FE} \overset{def}{=} (A_1)^{(0)}$	$(A_1)^{(1)}$	$(A_1)^{(2)}$	$(A_1)^{(3)}$	$(A_1)^{(4)}$
0.2	1.345310				
0.1	1.471463	2.581315			
0.05	1.604977	2.779589	3.604857	2.810813	
0.025	1.736848	2.896100	3.385695	2.827397	2.855389
0.01	1.900159	2.967961	3.217832		

6. Discussion and conclusions

A technique for extracting thermal generalized stress intensity factors in two-dimensional domains is presented. It is based on the modified Steklov formulation for computing the eigen-pairs, the minimum complementary weak form, Richardson's extrapolation and the p-version of the finite element method. The results obtained are shown to be accurate and the technique being efficient, and most importantly, applicable to singularities associated with re-entrant corners, multi-material interfaces and anisotropic materials.

An important step in the development of the overall technique is understanding the structure of the particular stress tensor (due to the thermal loading), and its influence on the TGSIFs. The recognition of the behavior of the error in computing the TGSIFs when the particular stress tensor is not included in the statically admissible space enabled a simplified approach for extracting the TGSIFs in a limiting process. Otherwise, one had to explicitly compute $\boldsymbol{\sigma}_P$ and $\overline{\boldsymbol{\sigma}}_P$ and add them to the statically admissible space, resulting in a complicated and cumbersome numerical procedure.

Numerical experiments for crack-tip singularities, and singularities associated with multi-material interfaces are presented. All experiments demonstrate that accurate TGSIFs can be extracted although the integration radii are large and away from the singular point. Thus, a strong mesh refinement in the vicinity of the singular point is not necessary for obtaining good results, enabling an efficient numerical procedure.

Acknowledgments

The reported work has been partially supported by the Government of Israel, Ministry of Absorption, Center for Science Absorption, and by the AFOSR under STTR/TS project No. FQ8671-9501469. The author thanks an anonymous referee for his valuable comments leading to improvements in the presentation of the paper and for pointing out a mistake in an early stage of the manuscript.

References

[1] T. Hattori, S. Sakata and G. Murakami, A stress singularity parameter approach for evaluating the interfacial reliability of plastic encapsulated LSI devices, J. Electronic Packaging 111 (1989) 243–248.
[2] K. Ikegami, Some topics of mechanical problems in electronic packaging, Adv. Electronic Packaging, ASME-EEP 1 (1992) 567–573.
[3] G.C. Sih, On the singular character of thermal stresses near a crack tip, Trans. ASME, J. Appl. Mech. 29 (1962) 587–589.
[4] N. Sumi and T. Katayama, Thermal stress singularities at tips of a Griffith crack in a finite rectangular plate, Nucl. Engrg. Des. 60 (1980) 389–394.
[5] C-H. Tsai and C-C. MA, Thermal weight function of cracked bodies subjected to thermal loading, Engrg. Fract. Mech. 41(1) (1992) 27–40.
[6] M. Frankle, D. Munz and Y.Y. Yang, Stress singularities in a bimaterial joint with inhomogeneous temperature distribution, Int. J. Solids Struct. 33(14) (1996) 2039–2054.
[7] C-C. Ma, Plane solution of thermal stresses for anisotropic bimaterial elastic wedges, J. Thermal Stresses 18 (1995) 219–245.
[8] M.M. Michael and R.J. Hartranft, Thermal stress singularities in microelectronic, in: Proceedings—41st Electronic Components & Technology Conference, Atlanta, GA, USA (IEEE, Piscataway, NJ, 1991) 273–277.
[9] Z. Yosibash and B.A. Szabó, Numerical analysis of singularities in two-dimensions. Part 1: Computation of eigenpairs, Int. J. Numer. Methods Engrg. 38(12) (1995) 2055–2082.

[10] B.A. Szabó and Z. Yosibash, Numerical analysis of singularities in two-dimensions. Part 2: Computation of the generalized flux/stress intensity factors, Int. J. Numer. Methods Engrg. 39(3) (1996) 409–434.
[11] Z. Yosibash, Numerical thermo-elastic analysis of singularities in two-dimensions. Int. J. Fracture 74(4) (1996) 341–361.
[12] C. Susanne Brenner and L. Ridgway Scott, The Mathematical Theory of Finite Element Methods (Springer-Verlag Publishers, Berlin, Heidelberg, New York, 1994).
[13] B.A. Szabó and I. Babuška, Finite Element Analysis (John Wiley & Sons, New York, 1991).
[14] P. Grisvard, Elliptic Problems in Nonsmooth Domains (Pitman Publishing, UK, 1985).
[15] D. Leguillon and E. Sanchez-Palencia, Computation of Singular Solutions in Elliptic Problems and Elasticity (John Wiley & Sons, New York, NY, 1987).
[16] D. Gilbarg and N.S. Trudinger, Elliptic Partial Differential Equations of Second Order (Springer-Verlag, Publishers, Berlin, Heidelberg, New York, 1977).
[17] J. Nečas and I. Hlaváček, Mathematical Theory of Elastic and Elastico-plastic Bodies: An Introduction (Elsevier, Amsterdam-Oxford-New York, 1981).
[18] A. Ralston and P. Rabinowitz, A First Course in Numerical Analysis, 2nd edition (McGraw-Hill, New York, USA, 1977).
[19] N.N.V. Prasad, M.H. Aliabadi and D.R. Rooke, The dual boundary element method for thermoelastic crack problems, Int. J. Fracture 66 (1994) 255–272.
[20] K. Lee and Y.H. Cho, Boundary element analysis of thermal stress intensity factors for cusp cracks, Engrg. Fract. Mech. 37(4) (1990) 787–798.
[21] N. Liu and J. Altiero, A new boundary element method for the solution of plane steady-state thermoelastic fracture mechanics problems, Appl. Math. Modell. 16 (1992) 618–628.
[22] S. Nakanishi, S. Tani, M. Suzuki and N. Sumi, Orthotropic rectangular plates with an eccentric crack and an inclined crack in steady state temperature fields, Trans. Japan Soc. Mech. Engrs. 51(469) (1985) 2094–2102 (in Japanese).
[23] Y. Murakami, Stress Intensity Factors Handbook, Two volumes (Pergamon Press, New York, NY, 1987).
[24] Dai-Heng Chen, Analysis of singular stress field around the inclusion corner tip, Engrg. Fract. Mech. 49(4) (1994) 533–546.